Electronic Supplementary Material (ESI) for Lab on a Chip.

Portable platform for leukocyte extraction from blood using sheath-free microfluidic DLD

Oriana Chavez-Pineda[1], Roberto Rodriguez-Moncayo[1], Alan M. Gonzalez-Suarez[1], Pablo E. Guevara-Pantoja[1], Jose L. Maravillas-Montero[2] and Jose L Garcia-Cordero[1,3]*

[1]Laboratory of Microtechnologies Applied to Biomedicine (LMAB), Centro de Investigación y de Estudios Avanzados (Cinvestav), Monterrey, NL, Mexico

[2]Red de Apoyo a la Investigación, Universidad Nacional Autónoma de México e Instituto Nacional de Ciencias Médicas y Nutrición Salvador Zubirán, Mexico City14080, Mexico

[3] Institute of Human Biology (IHB), Roche Pharma Research and Early Development, Roche Innovation Center Basel, Basel 4058, Switzerland.

*Corresponding author: jose_luis.garcia_cordero@roche.com

Movie S1.

Real-time movie of leukocyte separation from a blood sample with Hct 6%at a flow rate of 2 µL/min. WBCs (stained with Hoechst) can be observed traveling in the center of the channel while erythrocytes move close to the channel walls.

Table S1. List of reported DLD microfluidic devices for blood cell isolation.

Applications	# Inlets	Sheath	Flow rate	Efficiency	Purity	Viability	Ref.
Separation of WBCs and RBCs	3	Yes	0.4 - 1 µL/min	99%	N/S	N/S	2006[1]
Separation of parasites from human blood	3	Yes	1 nL/ min	99.6%	N/S	N/S	2011[2]
Separation of RBCs with differing deformability and isolation of WBCs	3	Yes	N/S	99%	N/S	N/S	2014[3]
Enrichment of circulating tumor cells	2	Yes	N/S	88%	N/S	99%	2015[4]
Separation WBCs and mechanical protein extraction	2	Yes	N/S	99%	72%	N/S	2015[5]
Separation of WBCs	2	Yes	10 µL/min	99%	N/S	N/S	2016[6]
Enrichment of WBCs from blood	1	No	115 µL/ min	98.7%	N/S	N/S	2011[7]
Separation of cancer cells from blood	1	No	mL/ min	86%	N/S	96%	2012[8]
Isolation of cancer cells from blood	1	No	~mL / min	99%	N/S	N/S	2013[9]
Separation of parasites from human blood	1	No	0.25 - 3.8 µL/min	leukocyte 99% parasites 67.9	N/S	N/S	2016[10]
Separation of particle/cell	1	No	83 µL/min	~ 99%	Particle ~98% Cells ~18%	N/S	2020[11]
Separation of particles/cells	3	Yes	1-4 µL/min capillary pressure	Particles 94-98% Cells 99.65-99.98%	N/S	N/S	2023[12]

N/S: Not specified.

Table S2. Dimensions of focusing structures simulated in COMSOL.

Focusing structures	Width (μm)	Side (μm)	Side (μm)	Side(μm)	Side (μm)	Side (μm)
1 Trapezoid	1500	320	1100	1100	---	---
2 Trapezoid	2000	320	1300	1300	---	---
1 Hexagon	1400	320	1100	1100	1100	1100
2 Hexagon	1900	1200	345	345	950	950
3 Hexagon	2600	1400	345	345	1200	1200

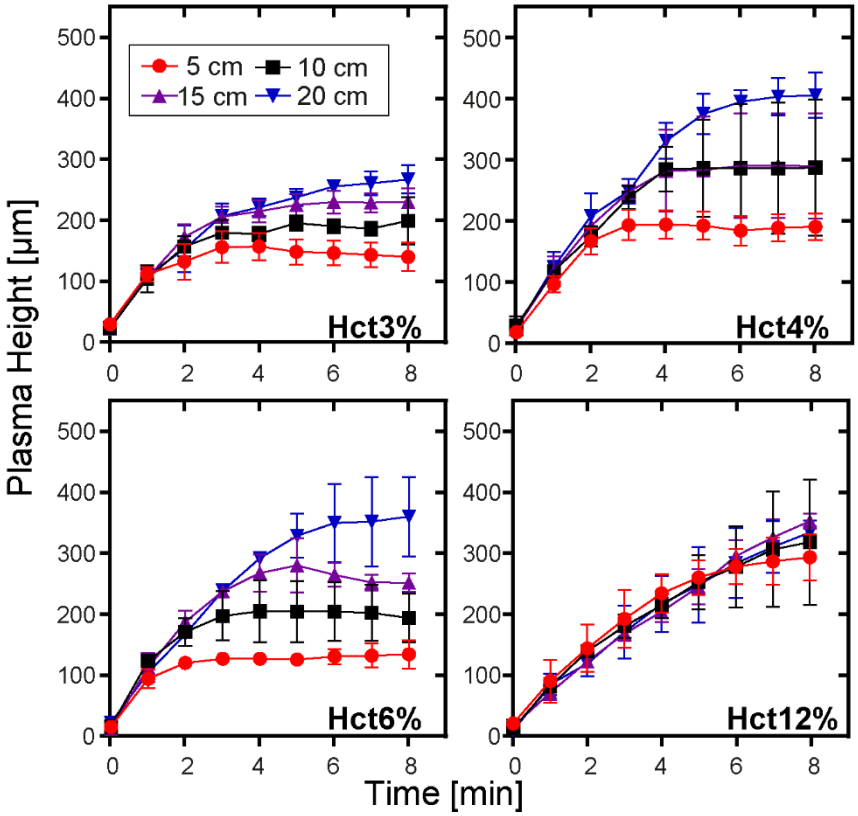

Figure S1. Plots show plasma height as a function of time for samples injected at different hematocrit levels (3%, 4%, %, and 12% Hct) at a flow rate of 4 μL/min and different distances from the tube (5, 10, 15, and 20 cm). Error bars indicate standard deviation (n = 3).

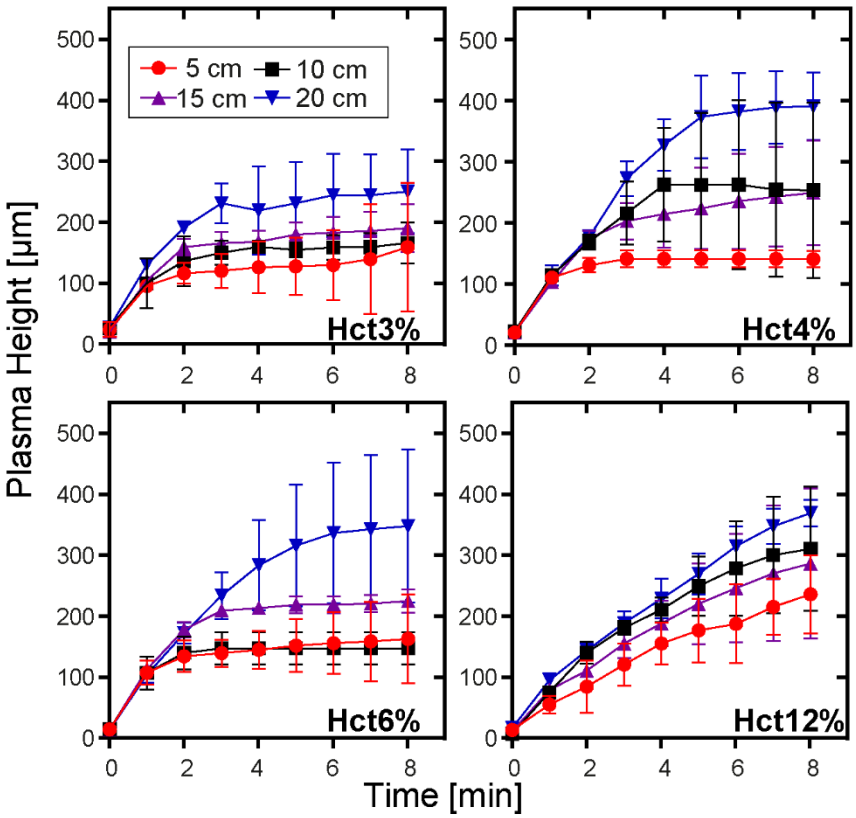

Figure S2. Plots show plasma height as a function of time for samples injected at different hematocrit levels (3%, 4%, 6%, and 12% Hct) at a flow rate of 6 µL/min and different distances from the tube (5, 10, 15, and 20 cm). Error bars indicate standard deviation (n = 3).

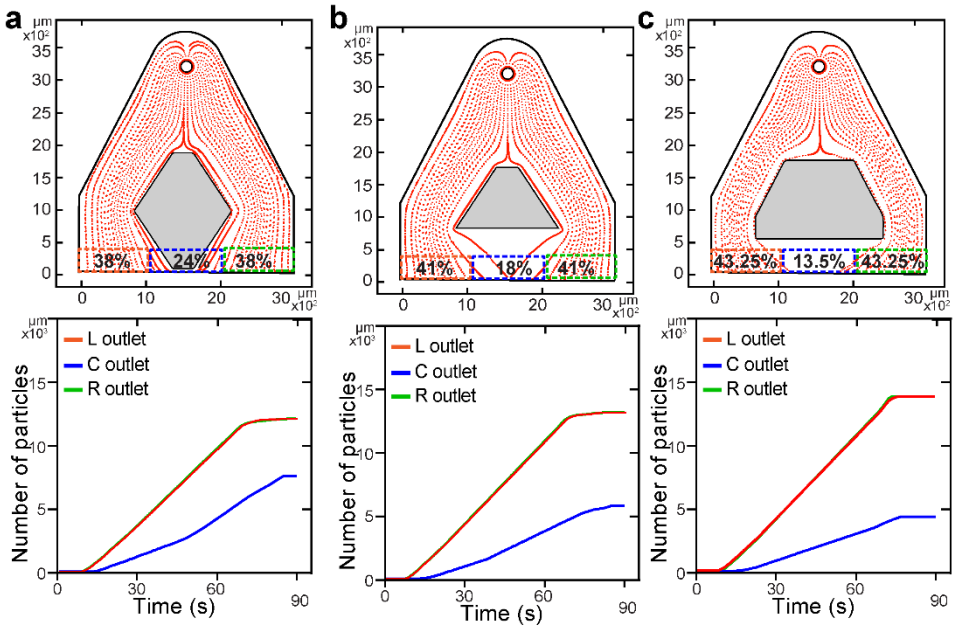

Figure S3. Simulations of particle trajectories at the inlet and plots showing particles exiting through the left (L), center (C), and right (R) outlets for devices with (**a**) a hexagonal focusing structure, (**b**) a trapezoidal focusing structure, and (**c**) an irregular hexagonal focusing structure.

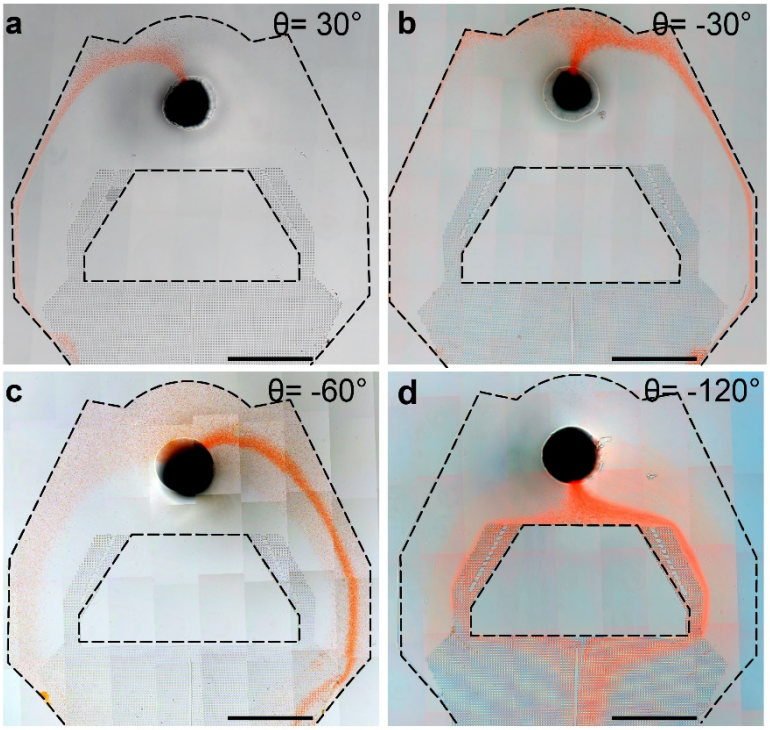

Figure S4. Sample focusing in the device with irregular hexagonal focusing structure at different interfacing tubing angles of (**a**) 30°, (**b**) -30°, (**c**) -60°, and (**d**) -120°. Scale bar is 1 mm.

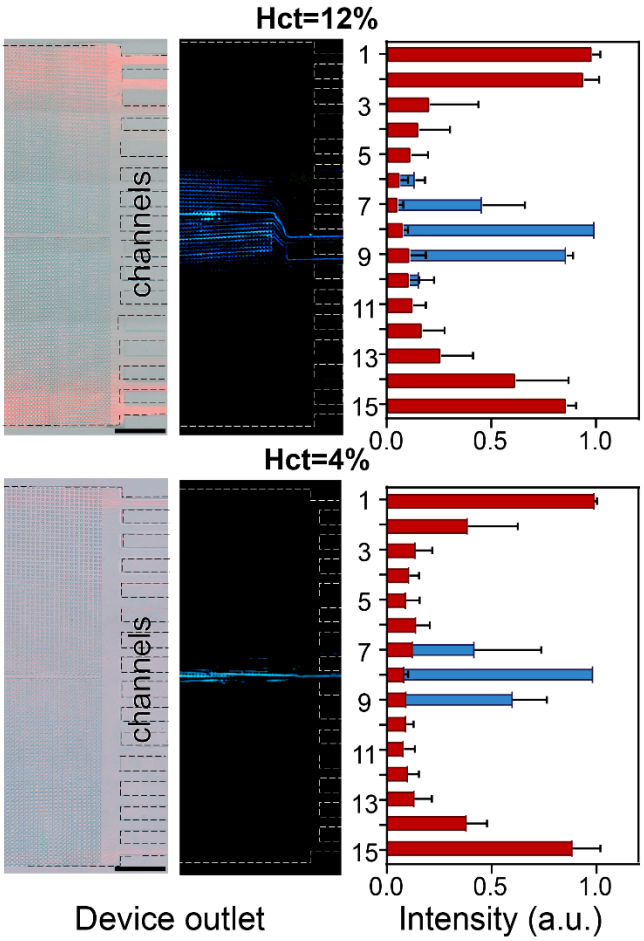

Figure S5. Influence of hematocrit on the distribution of WBCs and RBCs at the outlet of the DLD device. (Left panel) Brightfield and fluorescence micrographs showing the distribution of blood cells in the output channels when injecting samples with hematocrits of 12% and 4%. Scale bar is 400 μm. (Right panel) Bar graphs showing the highest gray level representing RBCs (red bars) and fluorescence intensity representing Hoechst-stained WBCs (blue bars) for samples with hematocrits of 12% and 4%.

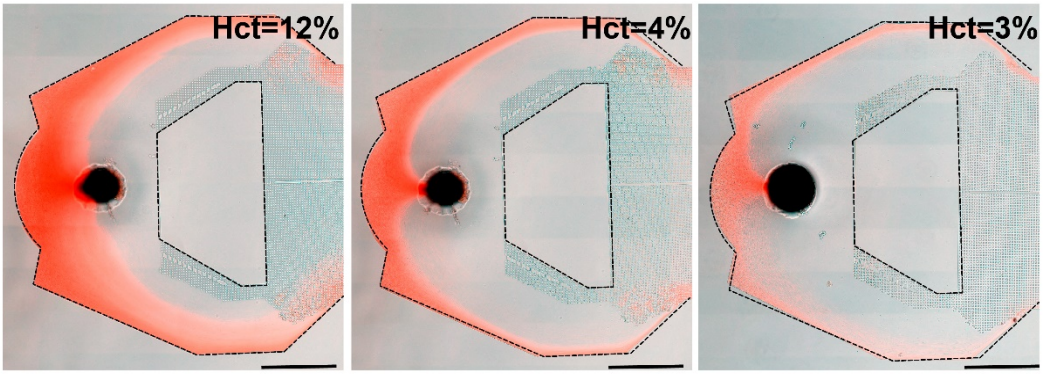

Figure S6. Micrographs of the DLD device inlet demonstrating the focusing of blood cells when injecting samples with different hematocrit percentages (12%, 4%, and 3% Hct). Scale bar is 1 mm.

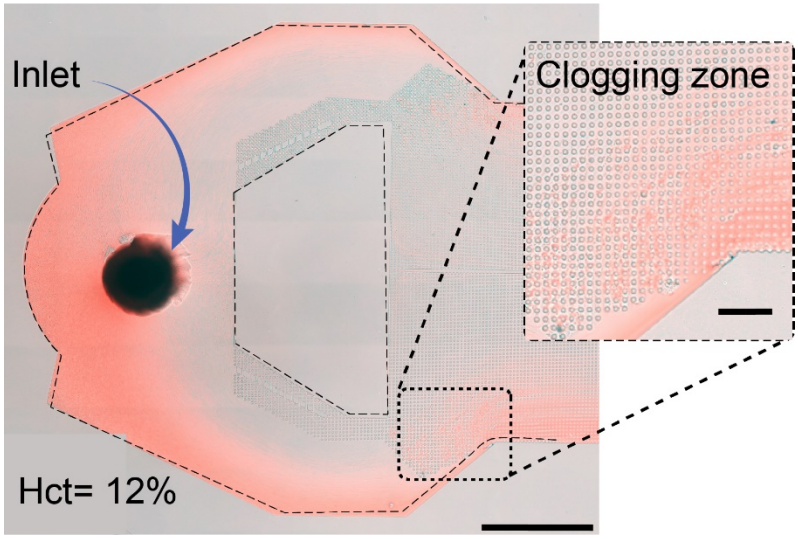

Figure S7. Micrograph of the device inlet revealing the obstruction of regions near the channel wall after 30 minutes of injecting a blood sample with 12% Hct. Scale bar is 1 mm. Magnified view of the occluded regions with blood cells. Scale bar is 200 μm.

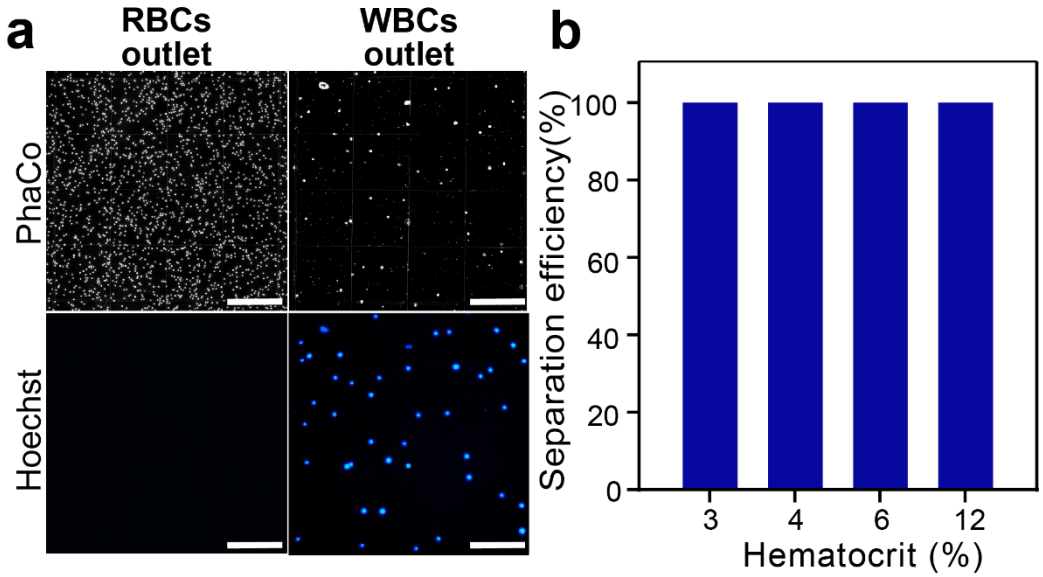

Figure S8. WBC separation efficiency for samples at different hematocrit percentages (3%, 4%, 6%, and 12% Hct). (**a**) Phase contrast (PhaCo) and fluorescence (Hoechst) micrographs of samples recovered at WBCs and RBCs outlet. Scale bar is 250 µm. (**b**) Plot showing WBC separation efficiency for samples with different hematocrit percentages.

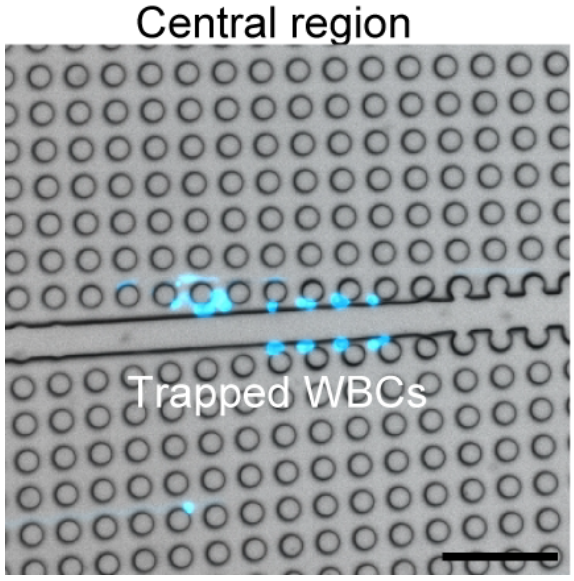

Figure S9. Micrograph of the central region of the device revealing leukocyte trapping between the posts and the central wall. Scale bar is 100 µm.

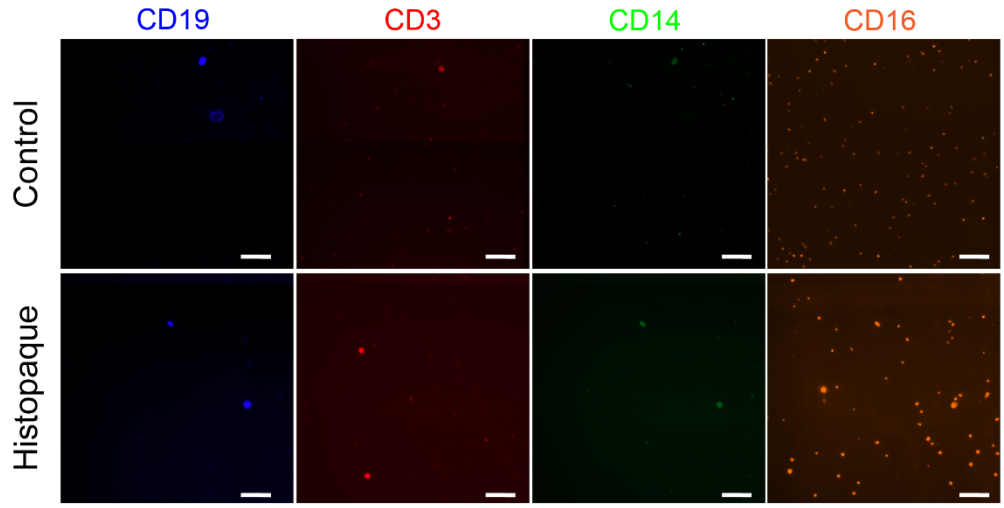

Figure S10. Fluorescence microscopy images of control WBCs and WBCs isolated by the Histopaque gradient, stained with surface markers (scale bar: 50 μm): polymorphonuclear (CD16), monocytes (CD14), T cells (CD3), and B cells (CD19).

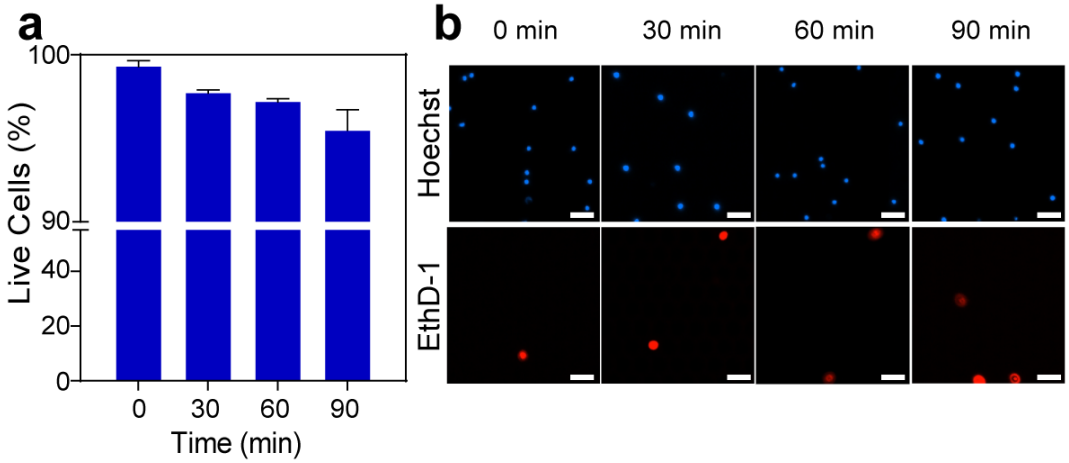

Figure S11. Viability of the WBCs sample recovered at the device output. (a) Plot shows the percentage of viable WBCs over time. (b) Representative fluorescence images of the viability assay showing all WBCs (Hoechst^{+}) and dead cells (EthD-1^{+}) at 0, 30, 60, and 90 min after isolation. Scale bar: 100 μm.

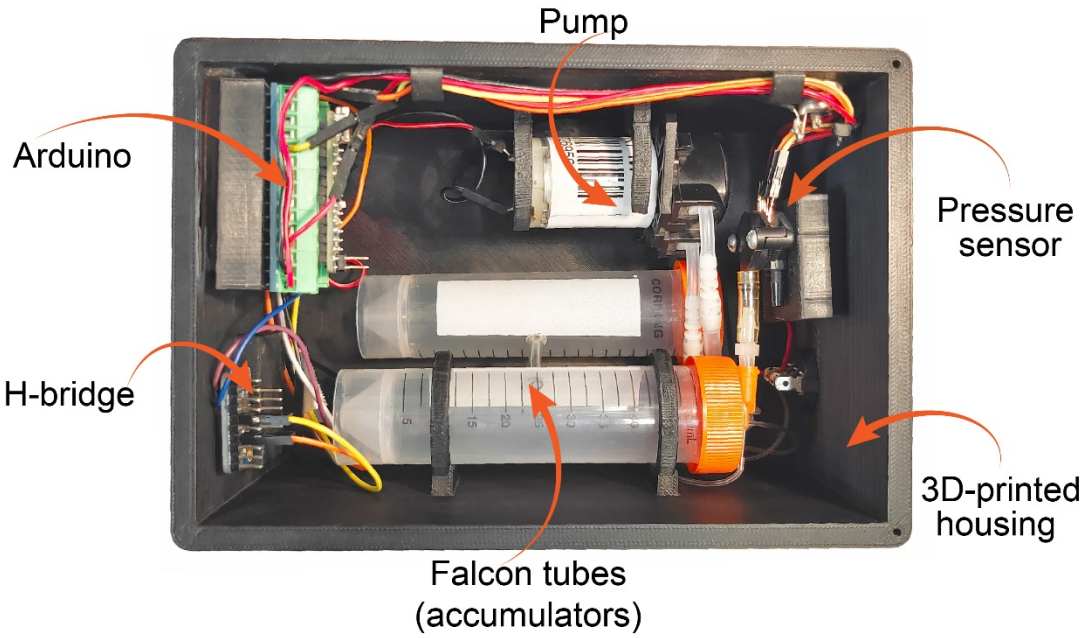

Figure S12. Photograph of the components inside the pressure system. The components are a small peristaltic pump, a microcontroller, a pressure sensor, two Falcon tubes, and an H-bridge.

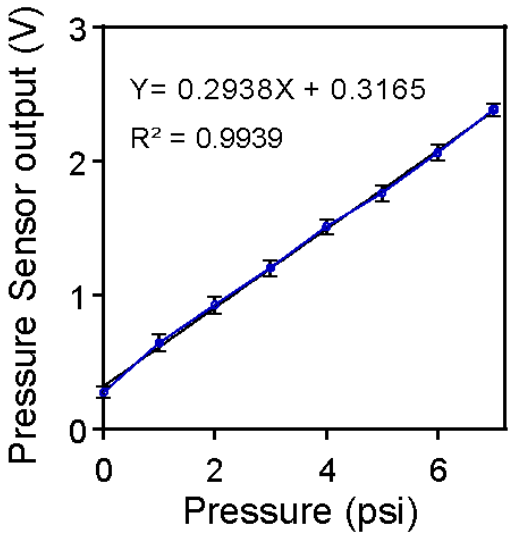

Figure S13. Calibration curve of the pressure sensor signal. We obtained a calibration curve in the range of 0 to 7 psi to convert the values collected by the pressure sensor. The calibration curve equation permits us to configure a program in an Arduino microcontroller to achieve the required pressures.

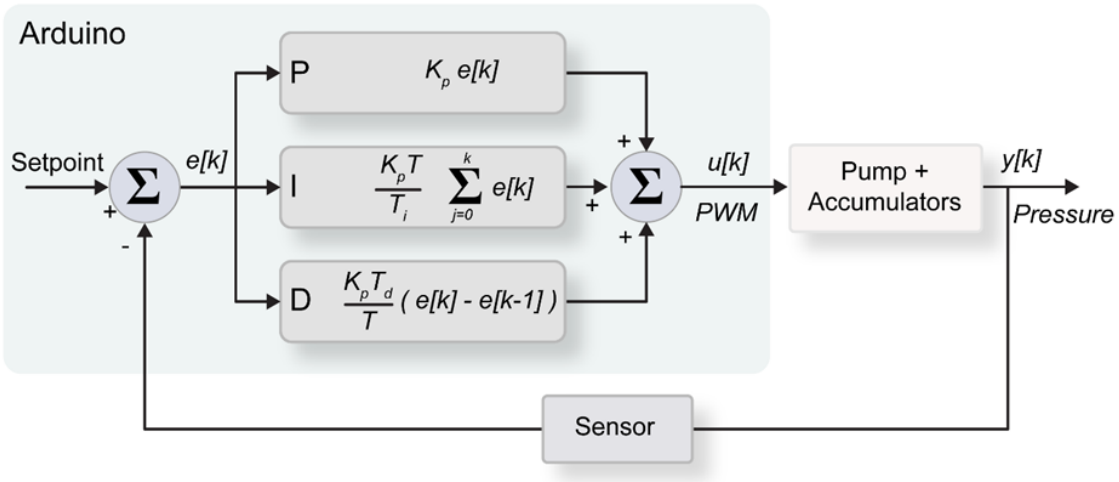

Figure S14. Block diagram of the digital PID controller implemented with Arduino. Where *e* is the error, *k* is the iteration, *u* is the controller output, *y* is the pressure, *T* is the sampling time, and K_p, K_p/T_i, K_pT_d are the proportional, integrative, and derivative constants respectively.

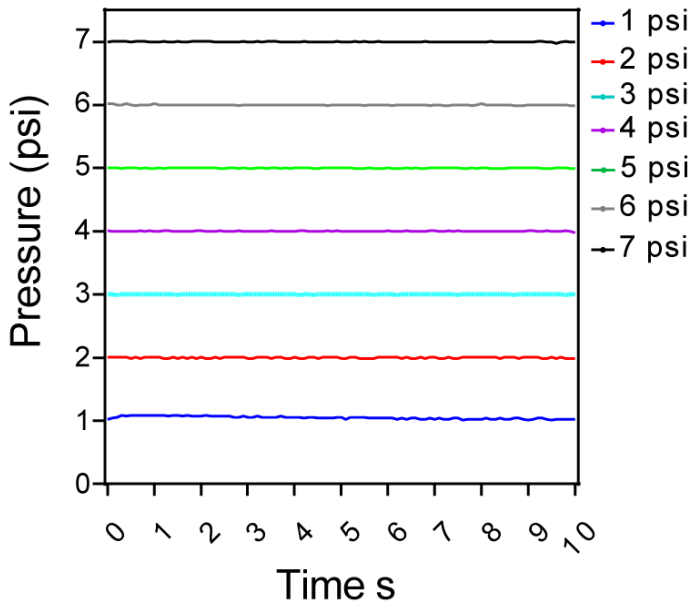

Figure S15. System characterization at different pressures.

References

(1) Davis, J. a; Inglis, D. W.; Morton, K. J.; Lawrence, D. a; Huang, L. R.; Chou, S. Y.; Sturm, J. C.; Austin, R. H. Deterministic Hydrodynamics: Taking Blood Apart. *Proc Natl Acad Sci U S A* **2006**, *103* (40), 14779–14784. https://doi.org/10.1073/pnas.0605967103.

(2) Holm, S. H.; Beech, J. P.; Barrett, M. P.; Tegenfeldt, J. O. Separation of Parasites from Human Blood Using Deterministic Lateral Displacement. *Lab Chip* **2011**, *11* (7), 1326–1332. https://doi.org/10.1039/c0lc00560f.

(3) Holmes, D.; Whyte, G.; Bailey, J.; Vergara-Irigaray, N.; Ekpenyong, A.; Guck, J.; Duke, T. Separation of Blood Cells with Differing Deformability Using Deterministic Lateral Displacement. *Interface Focus* **2014**, *4* (6). https://doi.org/10.1098/rsfs.2014.0011.

(4) Okano, H.; Konishi, T.; Suzuki, T.; Suzuki, T.; Ariyasu, S.; Aoki, S.; Abe, R.; Hayase, M. Enrichment of Circulating Tumor Cells in Tumor-Bearing Mouse Blood by a Deterministic Lateral Displacement Microfluidic Device. *Biomed Microdevices* **2015**, *17* (3), 1–11. https://doi.org/10.1007/s10544-015-9964-7.

(5) Choi, J.; Hyun, J. C.; Yang, S. On-Chip Extraction of Intracellular Molecules in White Blood Cells from Whole Blood. *Sci Rep* **2015**, *5*, 1–12. https://doi.org/10.1038/srep15167.

(6) Civin, C. I.; Ward, T.; Skelley, A. M.; Gandhi, K.; Peilun Lee, Z.; Dosier, C. R.; D'Silva, J. L.; Chen, Y.; Kim, M. J.; Moynihan, J.; Chen, X.; Aurich, L.; Gulnik, S.; Brittain, G. C.; Recktenwald, D. J.; Austin, R. H.; Sturm, J. C. Automated Leukocyte Processing by Microfluidic Deterministic Lateral Displacement. *Cytometry Part A* **2016**, *89* (12), 1073–1083. https://doi.org/10.1002/cyto.a.23019.

(7) Inglis, D. W.; Lord, M.; Nordon, R. E. Scaling Deterministic Lateral Displacement Arrays for High Throughput and Dilution-Free Enrichment of Leukocytes. *Journal of Micromechanics and Microengineering* **2011**, *21* (5). https://doi.org/10.1088/0960-1317/21/5/054024.

(8) Loutherback, K.; D'Silva, J.; Liu, L.; Wu, A.; Austin, R. H.; Sturm, J. C. Deterministic Separation of Cancer Cells from Blood at 10 ML/Min. *AIP Adv* **2012**, *2* (4). https://doi.org/10.1063/1.4758131.

(9) Liu, Z.; Huang, F.; Du, J.; Shu, W.; Feng, H.; Xu, X.; Chen, Y. Rapid Isolation of Cancer Cells Using Microfluidic Deterministic Lateral Displacement Structure. *Biomicrofluidics* **2013**, *7* (1). https://doi.org/10.1063/1.4774308.

(10) Holm, S. H.; Beech, J. P.; Barrett, M. P.; Tegenfeldt, J. O. Simplifying Microfluidic Separation Devices towards Field-Detection of Blood Parasites. *Analytical Methods* **2016**, *8* (16), 3291–3300. https://doi.org/10.1039/c6ay00443a.

(11) Tottori, N.; Nisisako, T. Particle/Cell Separation Using Sheath-Free Deterministic Lateral Displacement Arrays with Inertially Focused Single Straight Input. *Lab Chip* **2020**, *20* (11), 1999–2008. https://doi.org/10.1039/D0LC00354A.

(12) Aghajanloo, B.; Ejeian, F.; Frascella, F.; Marasso, S. L.; Cocuzza, M.; Tehrani, A. F.; Nasr Esfahani, M. H.; Inglis, D. W. Pumpless Deterministic Lateral Displacement Separation Using a Paper Capillary Wick. *Lab Chip* **2023**, *23* (8), 2106–2112. https://doi.org/10.1039/d3lc00039g.